T2R2 東京工業大学リサーチリポジトリ
Tokyo Tech Research Repository

論文 / 著書情報
Article / Book Information

Title	Superscattering from cylindrical hyperbolic metamaterials in the visible region
Authors	Rahul Kumar, Kotaro Kajikawa
Citation	Optics Express, Vol. 28, Issue 2, pp. 1507-1517
Pub. date	2020, 1
Copyright	(c) 2020 Optical Society of America. Users may use, reuse, and build upon the article, or use the article for text or data mining, so long as such uses are for non-commercial purposes and appropriate attribution is maintained. All other rights are reserved.
DOI	http://dx.doi.org/https://doi.org/10.1364/OE.379547

Powered by T2R2 (Tokyo Institute Research Repository)

Research Article | Vol. 28, No. 2 / 20 January 2020 / Optics Express 1507

Optics EXPRESS

Superscattering from cylindrical hyperbolic metamaterials in the visible region

RAHUL KUMAR AND KOTARO KAJIKAWA*

Department of Electrical and Electronic Engineering, School of Engineering, Tokyo Institute of Technology, Nagatsuta, Midori-ku, Yokohama, Kanagawa 226-8502, Japan
kajikawa@ee.e.titech.ac.jp

Abstract: We report that cylindrical hyperbolic metamaterials (CHMMs) exhibit superscattering (SSc) in the visible region, based on analytical and numerical calculations. It has normalized scattering cross-section (NSCS) twice as large as that from cylinders consisting of homogeneous materials. This large NSCS is due to constructive interference of multipolar resonances. Finite-difference time-domain calculations revealed that the spatial field-distribution at the SSc condition is similar to that of a whispering gallery mode (WGM), suggesting that the WGM-like field distribution is responsible for the large scattering. It is also reported that the SSc can be achieved in CHMM of epsilon near zero materials.

© 2020 Optical Society of America under the terms of the OSA Open Access Publishing Agreement

1. Introduction

Optical superscattering (SSc) from a subwavelength nanostructure is a phenomenon in which the scattering cross section exceeds the single-channel limit i.e. normalized scattering cross section (NSCS) is greater than unity [1], due to the constructive interference of multipolar resonances. It can be applied in sensing, spectroscopy, bio-medical imaging, energy harvesting and other applications which involve the manipulation of scattering of light [2]. Recent studies have demonstrated SSc from several structures, such as radially anisotropic nanowires [3,4], multilayered cavities [5], core-shell nanowires [6,7], nanospheres [8,9] and structures with phase-change materials [10,11]. In general, SSc is observed in a narrow spectral band, and depends strongly on the losses in the materials. Research in this area has become even more promising after a recent experimental demonstration in the microwave regime [12].

In this paper we predict SSc from cylindrical hyperbolic metamaterials (CHMMs) consisting of materials known to exist in the real world, at visible wavelengths. The CHMM is made up of metal and dielectric layers with a thickness of 6 – 30 nanometer. CHMMs have been widely studied for various applications, including invisibility [13], broadband absorption [14] and optical hyperlens [15,16]. We have briefly reported SSc from a CHMM [17], but no detailed mechanism or design of the CHMM have yet been reported. We report here the mechanism of SSc in suitably designed materials on the basis of analytical and numerical calculations. SSc is found to stem from constructive interference of the multipolar resonances. It was also found that the SSc condition is attained in CHMMs consisting of metallo-dielectric and epsilon-near-zero (ENZ) materials in the visible region. Our FDTD calculation shows that the spatial field distribution in the SSc condition is similar to a whispering gallery mode (WGM), suggesting that the WGM-like electric-field distribution leads to high scattering efficiency. WGM-like field distributions have been reported for spherical hyperbolic cavities in the infrared [18], and for a further metamaterial structure in the GHz region [19], but no study has yet been made for CHMM in the visible region. CHMMs are promising materials for SSc, and maybe applied in sensing, beam shaping, energy harvesting and other applications.

#379547 https://doi.org/10.1364/OE.379547
Journal © 2020 Received 2 Oct 2019; revised 22 Nov 2019; accepted 20 Dec 2019; published 10 Jan 2020

Optics EXPRESS

2. Calculation

The CHMM consists of a cylindrical core (permittivity $\varepsilon_{\text{core}}$ and a 50-nm radius ρ_{core}) coated alternately with multilayers of dielectrics (permittivity ε_{d}) and metals (permittivity ε_{m}), as shown in Fig. 1(a). All layers are taken to be of the same thickness, t. CHMM in which the core and the outermost layer material are silver is denoted CHMMm, and CHMM in which the core and outermost layer comprises dielectric is denoted CHMMd. The ambient permittivity ϵ_{amb} is set to unity. CHMM with 6 layers (three pairs of dielectric/metal layers) and t = 10 nm is the main focus of this analysis, because 6 layers is sufficient for SSc (see the next section). The z-axis is set along the long axis of the cylinder. The cylinder is assumed to be of infinite length, for simplicity. The light is incident along the x-axis. We consider transverse electric (TE) polarization (polarized in the y-direction) whereby the electric field has polarization along y-axis, because the SSc phenomenon is efficient only with incident TE polarization.

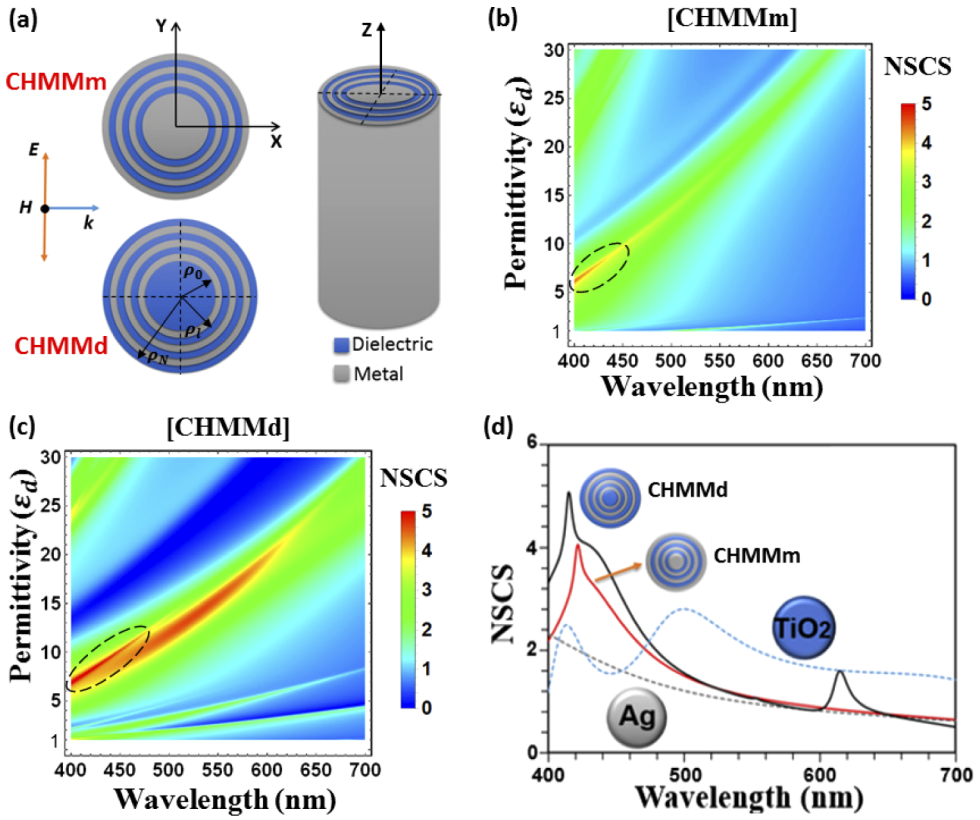

Fig. 1. (a) Schematics of CHMMm and CHMMd. Light with TE polarization is incident along the x-axis. (b) Density plot of NSCS as a function of wavelength and the dielectric permittivity (ε_d), for (b) CHMMm (c) CHMMd. (d) NSCS spectra for various cylinders of equal outer diameter 220 nm: CHMMd, CHMMm, silver and TiO_2.

For analytical calculations of the optical response from the CHMM, we used the Lorentz-Mie method with a transfer matrix approach [17,20–22]. The NSCS, σ, is considered as a figure of merit for scattering of subwavelength structures. For cylinders, it is calculated as $\sigma = \sum_{n=-\infty}^{+\infty} |d_n|^2$, where d_n is the scattering coefficient and n is the mode order. For the SSc phenomenon, σ>1. The detailed equations used for NSCS calculation are presented in Appendix A.

Optics EXPRESS

The numerical calculations were carried out according to the two-dimensional FDTD method, using the Lumerical FDTD Solutions, so as to obtain the electric field distribution. Conformal mesh type 1 was used, with a mesh size of 0.1 nm in each direction. A perfect-matched layer was taken as the boundary condition. The CHMM was illuminated by a pulse having a broadband light spectrum (400 nm to 700 nm). The permittivity of silver and TiO_2 is taken from the literature [17].

3. Results and discussion

3.1. Structures consisting of normal materials

We first consider the optical response of CHMMm, which has a silver core. Silver (Ag) was used because it is a metal having small imaginary permittivity. The dielectric material is determined as follows. Figure 1(b) shows a density plot of the NSCS of CHMMm as a function of wavelength and the permittivity (ε_d) of the dielectric material. When the dielectric permittivity is between 6 and 10, a narrow region of large NSCS (greater than 4) is observed, shown by the dashed line. CHMMm alone, at limited permittivity and wavelengths, exhibits SSc. There is no low-NSCS region (NSCS < 0.5), indicating that no invisible CHMMm is possible.

Figure 1(c) shows a density plot of the NSCS of CHMMd. In contrast to CHMMm, the high NSCS region (NSCS > 4) is large. The NSCS is particularly large for dielectric permittivity between 6 and 10 at wavelengths of 400 – 450 nm. A low-NSCS region (NSCS < 0.5) occupying a large area is also present, in which the CHMMd is invisible. Further investigation of the invisibility of the CHMM is in process and will be reported elsewhere. As titanium dioxide (TiO_2) has suitable permittivity for the SSc, we chose it as the dielectric material. Figure 1(d) summarizes the scattering spectra of different structures of the same dimension (outer diameter of 220 nm). Clearly, CHMMd and CHMMm show a scattering peak at about 420 nm, and the NSCS peak has around double the scattering intensity than that of bare silver or TiO_2 cylinders with the same diameter. Hence, we conclude that SSc can be achieved with CHMM.

Figures 2(a) and 2(b) show far-field radiation profiles of scattering for (a) CHMMd and (b) CHMMm, at the NSCS peak wavelengths of (a) 415 nm and (b) 422 nm. These are plotted as a function of radiation angle, and the direction of illumination is defined as 0 degree. The profiles were calculated by the FDTD method. They are shown together with the profiles for homogeneous TiO_2 and silver cylinders. These profiles show large forward scattering of CHMMd and CHMMm, relative to those from the homogeneous TiO_2 and silver cylinders. The unidirectional enhanced scattering (for angles around 0 degree) from CHMM is suitable for nano antennas and scatterers for random lasers.

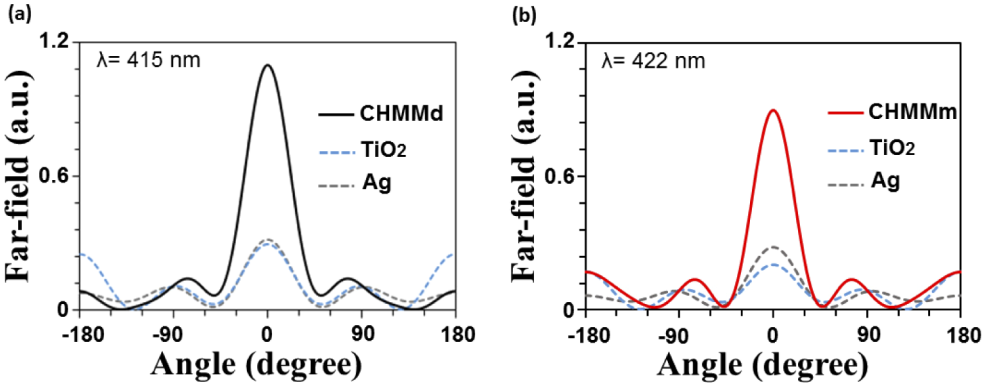

Fig. 2. Comparison of far field radiation patterns for (a) CHMMd at 415 nm and (b) CHMMm at 422 nm.

Optics EXPRESS

Figures 3(a) and 3(b) show NSCS spectra for differing numbers of layers (2 – 10 layers), N, so as to find the necessary number of layers for (a) CHMMd and (b) CHMMm. The total thickness of the shell, T, is fixed at 60 nm so that the thickness of each layer is T/N. Upon increasing the number of layers N from 2 to 6, the scattering spectra change and the magnitude increases. Further increase of N above 6 does not lead to any significant change in the spectra in either the CHMMd or CHMMm profile. We conclude that the optimum number of layers is 6 for achieving enhanced scattering.

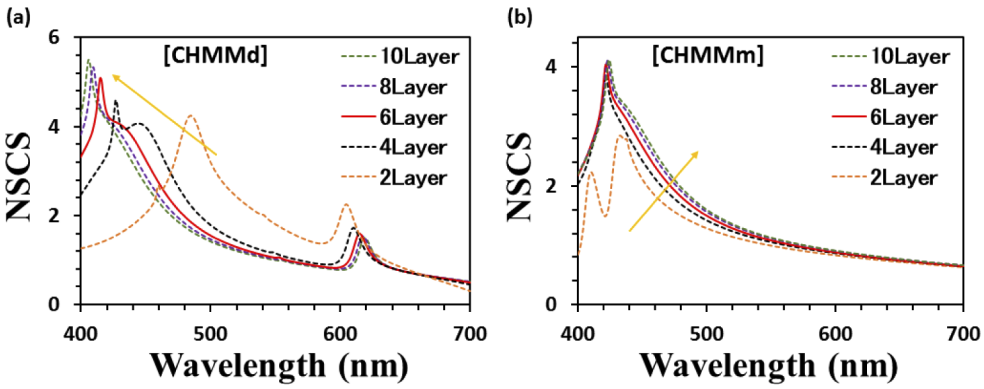

Fig. 3. Analysis of NSCS for differing numbers of layers in the CHMM shell structure. (a) CHMMd and (b) CHMMm.

The NSCS enhancement can be explained by degenerate resonances and by overlapping of different resonance modes of confined surface waves, such as the magnetic dipole mode ($n = 0$), and the electric dipole ($n = \pm 1$) and electric quadrupole ($n = \pm 2$) and other higher modes, as discussed in previous reports [1,3]. Figures 4(a) and 4(b) show the overlapping of different modes of resonances for CHMMd and for a homogeneous TiO_2 cylinder. The peak of the CHMMd at wavelength 415 nm is composed of overlapping modes with $n = \pm 1$, $n = \pm 2$ and $n = \pm 3$. This overlap results in significant enhancement of the NSCS (> 5). There is no such multipolar interference for the homogeneous TiO_2 cylinder. CHMM allows us to tune the different resonant modes so as to achieve enhanced scattering. Additionally, CHMM with an air core can also show SSc by following the same mechanism. [13,17] Moreover, some reports have analyzed the scattering property of plasmonic nanostructure [23] and graphene based superscatterers [24] using Bohr model, which is a phenomenological model. However, it was found that the model is more applicable to the graphene based superscatterers due to ease of determining the effective radius. Hence, we think that it is tedious to apply the Bohr model for our structure, considering the complexity of determining the effective radius for the multi-layered structure and the limitations of the model.

Furthermore, we obtained the electric field distribution of the CHMMd structure at wavelengths of 415, 500 and 615 nm (indicated by arrows in Fig. 4(a)). The field distribution at 415 nm is similar to that of WGM [25], for which the electric field is localized at the outer surface and has low mode volume with the hexapolar symmetry, like the WGM at mode order $q = 3$. A detailed analysis is given by Chihhui Wu *et al* [18] for WGM in hyperbolic cavities operating in the near infrared region, and by Diaz-Rubio *et al* [19] for metamaterial structures operating in the GHz region. CHMMd supports WGM of symmetry $q = 3$ irrespective of the smaller size and possibility of enhancement of photonic density of states. Existence of WGM like surface waves at the SSc condition can also be related to the non-Rayleigh diverging scattering behaviour observed in the anisotropic cylinders [26]. However electric field distribution at 500 nm, shown in Fig. 4(d), is mostly on the surface as if it behaves as a metallic cylinder. At 615 nm the field is

Optics EXPRESS

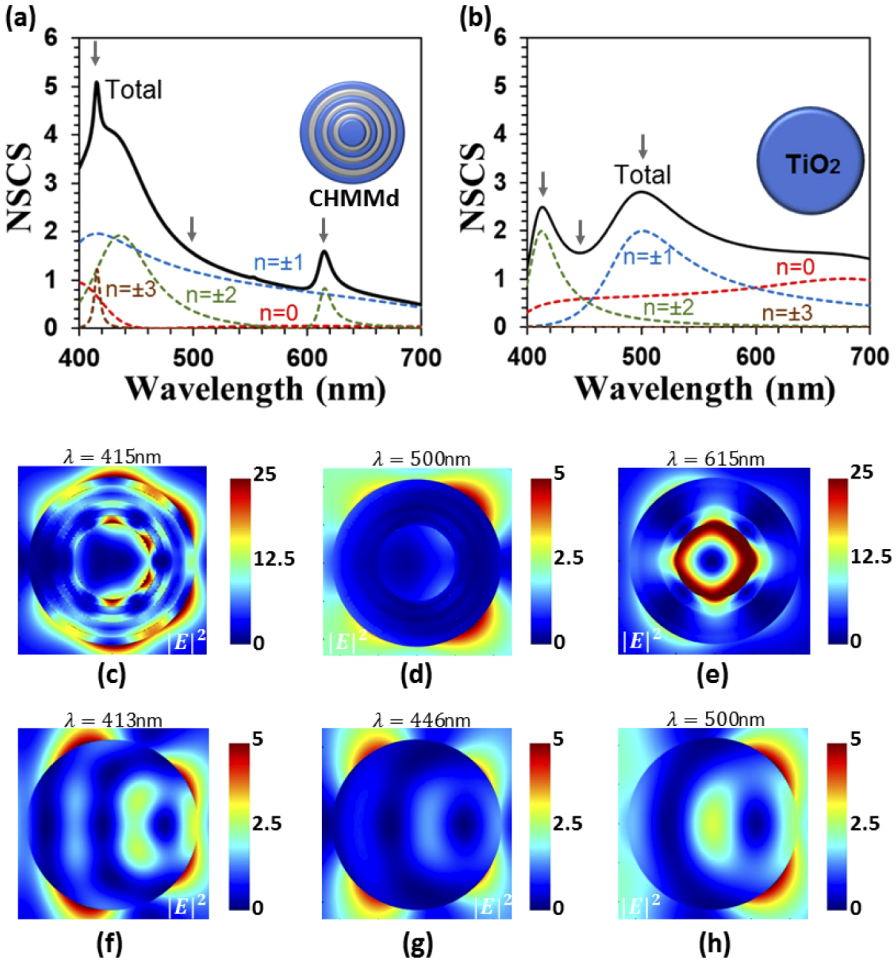

Fig. 4. Multi polar resonance modes of (a) CHMMd and (b) homogeneous TiO_2 cylinder. (c) Electric field ($|E|^2$) profile showing evidence of WGM of hexapolar symmetry ($q = 3$) at 415 nm, (d) $|E|^2$ distribution at 500 nm, (e) at 615 nm showing cavity mode with quadrupolar ($q = 2$) symmetry. $|E|^2$ profile for TiO_2 cylinder at different wavelengths (f) 413 nm, (g) 446 nm, and (h) 500 nm.

localized inside the core showing similarity to the cavity mode. The maximum magnitude of the electric field is lowest at a wavelength of 500 nm. Hence, it is concluded that CHMM can support multiple modes like WGM and cavity modes. For comparison we also show the electric field distributions in TiO_2 cylinder for different wavelengths shown in Figs. 4(f)–4(h). It can be observed that the strength of the field in TiO_2 is lower than at the SSc condition of CHMMd but comparable to that of at non-resonant (500 nm) case of CHMMd.

To design a CHMM for SSc, we calculate the NSCS of a structure comprising a cylindrical core (radius 50 nm) with alternate coatings of lossless materials of 10-nm thick layers A and B. The permittivity of the layers A and B is denoted ε_A and ε_B, respectively. CHMMd has a TiO_2 core and CHMMm has a silver core. Figures 5(a) and 5(b) are density plots of the NSCS of CHMMd and CHMMm at 415 and 422 nm, respectively, as a function of ε_A and ε_B, by which we can visualize the NSCS and consider the choice of the materials. CHMMd has regions of large NSCS, but CHMMm does not have such a high NSCS region. When CHMMd consists of metals and

Optics EXPRESS

dielectrics ($\varepsilon_A\varepsilon_B<0$), as shown in the second and fourth quadrants, a high NSCS region exists. The choice of the layer material, silver/TiO_2, is marked in the profile indicated as the intersection point of the dashed lines in Fig. 5(a), as $\mathrm{Re}(\varepsilon_{silver}) = -5.94$ (ignoring the imaginary part) and $\varepsilon_{TiO_2} = 7.84$. A narrow region with high NSCS is observed in the third quadrant, in which both ε_A and ε_B are negative, suggesting that SSc can be achieved with alternate deposition of metallic materials. Since the effective permittivity values for these combinations will be negative, the SSc observation can be related to the previous studies reporting anomalous diverging scattering condition for anisotropic cylinders [26,27].

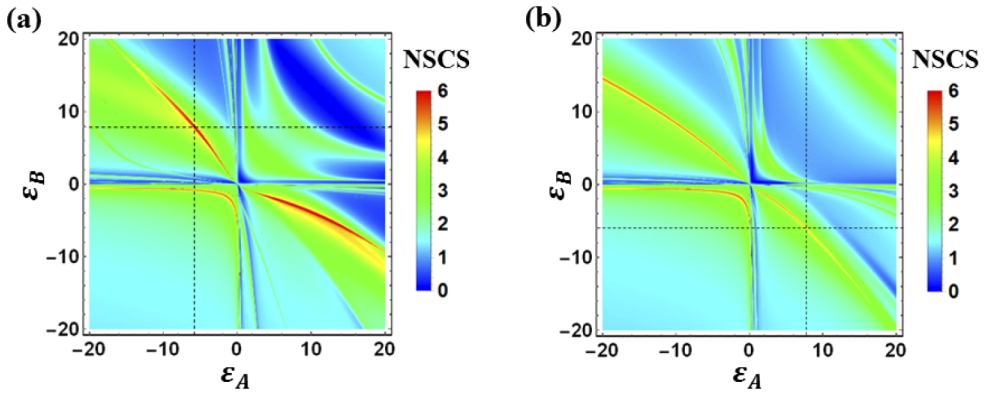

Fig. 5. NSCS profile as a function of ε_A and ε_B, for (a) CHMMd at 415 nm, and (b) CHMMm at 422 nm.

Both CHMMd and CHMMm have regions of low NSCS (less than 0.5). However, CHMMd has large area with low scattering region when compared to CHMMm. These regions correspond to low scattering phenomenon like invisibility, all dielectric cloaking [28] and plasmonic cloaking. The analysis confirms that the scattering property of CHMMd is tunable by appropriate design.

3.2. Structures consisting of ENZ materials

We now extend the SSc analysis to CHMM of alternate layers of silver and ENZ. We consider two kinds of structures with different core materials, one with Ag core is named as CHMMzm and the other with core of ENZ material is named as CHMMzz. ENZ materials have been studied previously in combination with high dielectric permittivity materials in cloaking applications [29,30], but SSc has not so far been reported for CHMM consisting of ENZ materials. Figure 6(a) shows a density plot of the NSCS for CHMMzm (structure shown in the inset of Fig. 6(c)) as a function of wavelength and the permittivity of ENZ, ε_{enz}. There are a few high NSCS branches (NSCS > 4). Similarly, NSCS is plotted for CHMMzz, although it shows areas with NSCS>1 but does not have high NSCS regions as present in CHMMzm. Based on this observation we will focus only on CHMMzm for SSc analysis. In addition we can notice that for CHMMzm and CHMMzz there exist large areas where NSCS is low. So, we can infer that structures consisting of ENZ materials along with metal can also exhibit very low scattering of light. This observation is different from the commonly reported structures of ENZ materials combined with high dielectric materials for cloaking applications [29,30].

To highlight the tuning capability of the CHMM, we set $\varepsilon_{enz} = 0.3$ and compare the scattering spectra with that of the homogeneous silver cylinder, in Fig. 6(b). The NSCS of CHMMzm is upto nearly four times that of the homogeneous silver cylinder at a wavelength near 500 nm. The resonance modes $n = 0, \pm1, \pm2$ and ±3 are also plotted. These overlap, and enhance the NSCS at 505 nm. The broad NSCS band is assigned to significant contributions of lower modes ($n = 0, \pm1, \pm2$) having broad peaks.

Optics EXPRESS

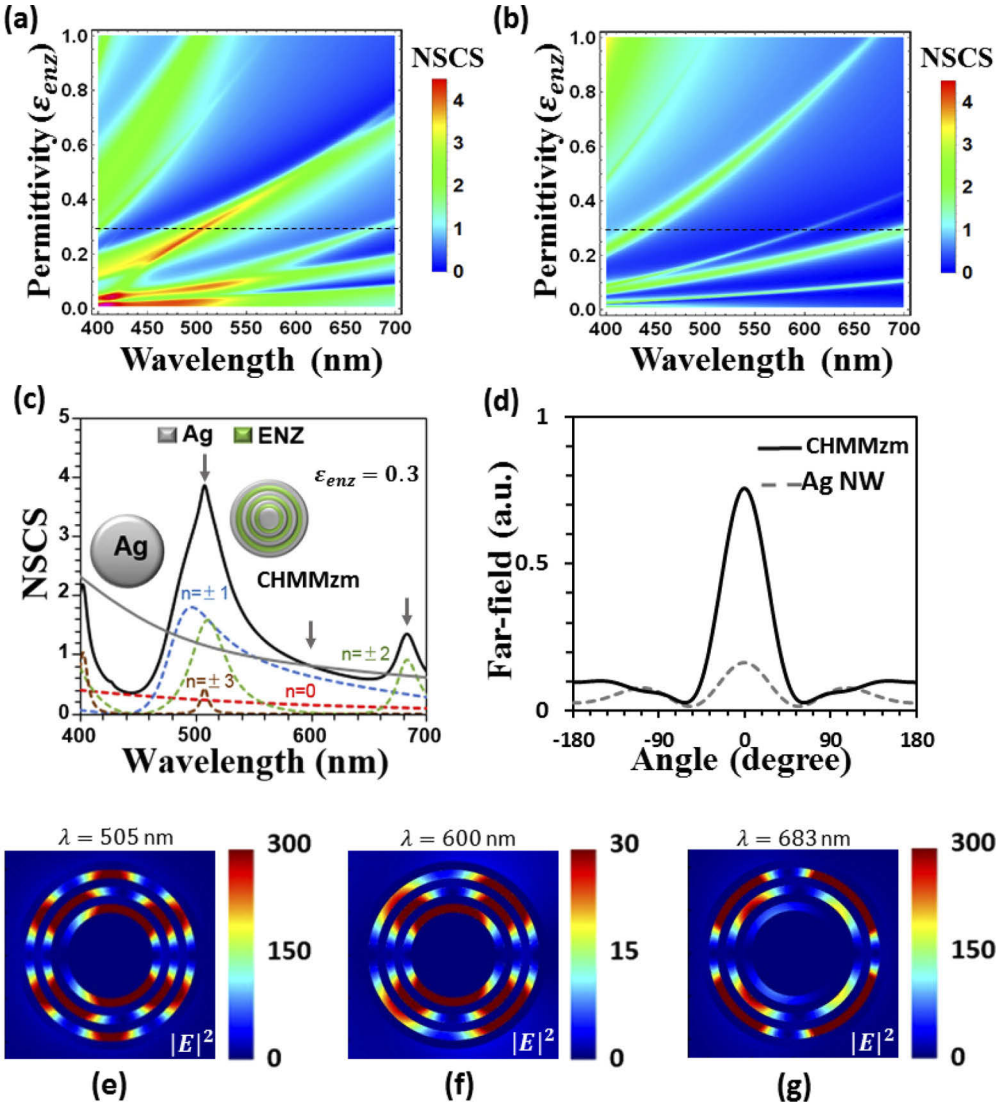

Fig. 6. SSc of CHMMs with ENZ material in CHMMz. (a) NSCS for different values of ε_{enz}, for CHMM based on Ag core (CHMMzm), where the dashed line represents $\varepsilon_{enz} = 0.3$ (b) NSCS for CHMMz with core of ε_{enz} (CHMMzz) (c) scattering spectra of the homogeneous silver cylinder and CHMMzm ($\varepsilon_{enz} = 0.3$), including multi polar modes of CHMMzm shown by dashed lines. (d) the far field of CHMMzm and the homogeneous silver cylinder at wavelength 505 nm. $|E|^2$ profiles for CHMMzm at different wavelengths showing drastic confinement of the field in the ENZ layers, for (e) 505 nm, 600 nm and 683 nm.

The electric field profile of CHMMzm at different wavelengths is shown in Figs. 6(e)–6(g). The electric field is strongly localized inside the thin layers of ENZ material, similar to the squeezing effect of the electromagnetic waves [31]. Additionally, the field intensity at resonant wavelengths (505 nm and 683 nm) are comparatively higher than at non-resonant condition (600 nm). In Fig. 6(d), we compare the far-field profile of CHMMz with that of the homogeneous silver cylinder at 505 nm. The profiles show unidirectional SSc in the ENZ-based metamaterials. Hence,

Optics EXPRESS

we have demonstrated that by using ENZ materials in CHMM we can achieve SSc behavior, and that the spectrum can be tuned by selecting ENZ materials of appropriate permittivity. Recently some promising materials such as Indium tin oxide, Titanium nitride etc. showing ENZ property were reported [32] which maybe helpful to realize ENZ materials based superscatterers in the visible region.

4. Conclusions

Enhancement of scattering using hyperbolic metamaterial structures has been demonstrated. The NSCS of CHMMd is twice that of the NSCS of a homogeneous cylinder. If we further use ENZ material, the enhancement factor is ~ 4. These SSc properties derive from constructive interference of the multipolar resonances. A finite-difference time-domain (FDTD) calculation shows that the spatial field distribution for the SSc phenomenon is similar to a whispering gallery mode (WGM). This finding strongly suggests that the WGM-like field distribution brings about the large scattering.

Appendix A. Details of calculation of NSCS

Following methodology is used to calculate the NSCS for the multi-layered structure (shown in Fig. 1(a)) when light is incident in TE-mode. The radius of the core is indicated as ρ_0, the distance of l-th layer from the center as ρ_l and of last layer as ρ_L. The magnetic field of the incident plane wave is expressed as,

$$H_{in} = \hat{z}H_0 \exp(ikx) = \hat{z}H_0 \sum_{n=-\infty}^{+\infty} i^n J_n(k\rho) \exp(in\phi) \tag{1}$$

where ρ and ϕ are the radial and azimuthal cylindrical coordinates, respectively, H_0 is a constant amplitude, J_n is the Bessel function of the first kind and order n, $k = k_0\sqrt{\varepsilon}$ and $k_0 = \omega/c$ is the wavenumber in the vacuum. The scattered magnetic field, for $\rho > \rho_L$, can be written as

$$H_{sca} = \hat{z}H_0 \sum_{n=-\infty}^{+\infty} d_n i^n H_n^{(1)}(k\rho) \exp(in\phi) \tag{2}$$

where $H_n^{(1)}$ is the Hankel function of the first kind and order n. The magnetic field in a given l-th layer of the CHMM (for $\rho_{l-1} < \rho < \rho_l$) can be expressed as,

$$H_l = \hat{z}H_0 \sum_{n=-\infty}^{+\infty} i^n [b_{n,l} J_n(k_l\rho) + c_{n,l} H_n^{(1)}(k_l\rho)] \exp(in\phi) \tag{3}$$

where $k_l = k_0\sqrt{\varepsilon_l}$. For $k_c = k_0\sqrt{\varepsilon_c}$, ε_c represents permittivity of the core medium, the magnetic field in the core of the structure can expressed as (for $\rho < \rho_0$)

$$H_c = \hat{z}H_0 \sum_{n=-\infty}^{+\infty} i^n d_n J_n(k_c\rho) \exp(in\phi) \tag{4}$$

The coefficients a_n, $b_{n,l}$, $c_{n,l}$ and d_n are determined by applying boundary conditions for the continuity of electric and magnetic field between the layers. The boundary conditions between the layers, applied at $\rho = \rho_l$ can be expressed in the matrix form as

$$D_{n,l}(\rho_l). \begin{bmatrix} b_{n,l} \\ c_{n,l} \end{bmatrix} = D_{n,l+1}(\rho_l). \begin{bmatrix} b_{n,l+1} \\ c_{n,l+1} \end{bmatrix} \tag{5}$$

Optics EXPRESS

where the matrix $D_{n,l}$ can be explained as

$$D_{n,l}(\rho_l) = \begin{bmatrix} \varepsilon_l J_n(k_l\rho_l) & \varepsilon_l H_n^{(1)}(k_l\rho_l) \\ \sqrt{\varepsilon_l} J_n'(k_l\rho_l) & \sqrt{\varepsilon_l} H_n'^{(1)}(k_l\rho_l) \end{bmatrix} \tag{6}$$

J_n' and $H_n'^{(1)}$ denotes the derivative. We also define a matrix T_n,

$$T_n = \begin{bmatrix} T_{n,11} & T_{n,12} \\ T_{n,21} & T_{n,22} \end{bmatrix} \tag{7}$$

$$T_n = D_{n,1}(\rho_0).\{\prod_{l=1}^{L}[D_{n,l}(\rho_l)]^{-1}.D_{n,l+1}(\rho_l)\} \tag{8}$$

Relation between the scattering coefficients is expressed as,

$$\begin{bmatrix} a_n \\ d_n \end{bmatrix} = \frac{1}{T_{n,12}y - T_{n,22}x} \begin{bmatrix} -T_{n,11}T_{n,22} + T_{n,12}T_{n,21} \\ xT_{n,21} - yT_{n,11} \end{bmatrix} \tag{9}$$

where, $x = \varepsilon_c J_n(k_c\rho_0)$ and $y = \sqrt{\varepsilon_c} J_n'(k_c\rho_0)$. Finally, the NSCS is calculated as

$$\sigma = \sum_{n=-\infty}^{+\infty} |d_n|^2 \tag{10}$$

Appendix B. Effect of geometrical variations and material losses on SSc

It is evident from previous reports [4,12] that the practical realization of superscattering can be limited by the geometrical variations and presence of material losses. We analyzed our proposed CHMMd structure for these factors which is presented in Fig. 7. With the variation in the thickness of each layer in ML model the overall shell thickness varies which results in the shift of resonant position but the NSCS value is nearly same. Next we compare the NSCS of CHMMd by varying the material loss, where ξ is the imaginary part of the silver's permittivity ($\varepsilon_{Ag}' = Re[\varepsilon_{Ag}] + i * \xi$) which represents the material loss factor. From Fig. 7(b) deterioration of the SSc property with the increase in material loss is evident.

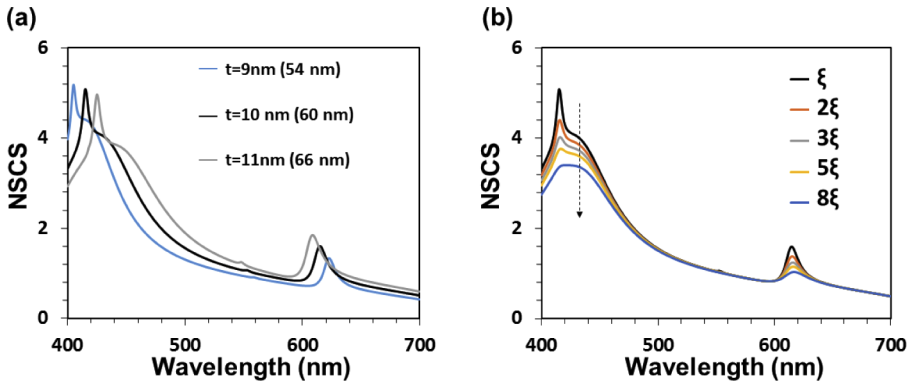

Fig. 7. (a) Effect of geometrical variation on the superscattering behaviour, values in parentheses denotes the overall thickness of shell (b) reduction of SSc performance with increase in material loss.

Optics EXPRESS

Funding

Japan Society for the Promotion of Science (16K13696, 19H02624, 26286058).

Acknowledgments

R. K. acknowledges financial support from the Japanese Government (MEXT) Scholarship.

Disclosures

The authors declare no conflicts of interest.

References

1. Z. Ruan and S. Fan, "Superscattering of light from subwavelength nanostructures," Phys. Rev. Lett. **105**(1), 013901 (2010).
2. F. Monticone, C. Argyropoulos, and A. Alù, "Multilayered plasmonic covers for comblike scattering response and optical tagging," Phys. Rev. Lett. **110**(11), 113901 (2013).
3. W. Liu, "Superscattering pattern shaping for radially anisotropic nanowires," Phys. Rev. A **96**(2), 023854 (2017).
4. C. Qian, X. Lin, Y. Yang, F. Gao, Y. Shen, J. Lopez, I. Kaminer, B. Zhang, E. Li, M. Soljačić, and H. Chen, "Multifrequency superscattering from subwavelength hyperbolic structures," ACS Photonics **5**(4), 1506–1511 (2018).
5. W. Liu, B. Lei, J. Shi, and H. Hu, "Unidirectional superscattering by multilayered cavities of effective radial anisotropy," Sci. Rep. **6**(1), 34775 (2016).
6. A. Mirzaei, A. E. Miroshnichenko, I. V. Shadrivov, and Y. S. Kivshar, "Superscattering of light optimized by a genetic algorithm," Appl. Phys. Lett. **105**(1), 011109 (2014).
7. A. Abrashuly and C. Valagiannopoulos, "Limits for absorption and scattering by core-shell nanowires in the visible spectrum," Phys. Rev. Appl. **11**(1), 014051 (2019).
8. Z. Ruan and S. Fan, "Design of subwavelength superscattering nanospheres," Appl. Phys. Lett. **98**(4), 043101 (2011).
9. Y. Huang and L. Gao, "Superscattering of light from core–shell nonlocal plasmonic nanoparticles," J. Phys. Chem. C **118**(51), 30170–30178 (2014).
10. Y. Huang, Y. Shen, C. Min, and G. Veronis, "Switching photonic nanostructures between cloaking and superscattering regimes using phase-change materials," Opt. Mater. Express **8**(6), 1672–1685 (2018).
11. S. Lepeshov, A. Krasnok, and A. Alù, "Nonscattering-to-superscattering switch with phase-change materials," ACS Photonics **6**(8), 2126–2132 (2019).
12. C. Qian, X. Lin, Y. Yang, X. Xiong, H. Wang, E. Li, I. Kaminer, B. Zhang, and H. Chen, "Experimental observation of superscattering," Phys. Rev. Lett. **122**(6), 063901 (2019).
13. K.-H. Kim, Y.-S. No, S. Chang, J.-H. Choi, and H.-G. Park, "Invisible hyperbolic metamaterial nanotube at visible frequency," Sci. Rep. **5**(1), 16027 (2015).
14. C. T. Riley, J. S. Smalley, J. R. Brodie, Y. Fainman, D. J. Sirbuly, and Z. Liu, "Near-perfect broadband absorption from hyperbolic metamaterial nanoparticles," Proc. Natl. Acad. Sci. U. S. A. **114**(6), 1264–1268 (2017).
15. A. V. Kildishev, U. K. Chettiar, Z. Jacob, V. M. Shalaev, and E. E. Narimanov, "Materializing a binary hyperlens design," Appl. Phys. Lett. **94**(7), 071102 (2009).
16. Z. Jacob, L. V. Alekseyev, and E. Narimanov, "Optical hyperlens: far-field imaging beyond the diffraction limit," Opt. Express **14**(18), 8247–8256 (2006).
17. R. Kumar and K. Kajikawa, "Comparison of cylinder-and planar-effective medium approximations on calculation of scattering properties of cylindrical hyperbolic metamaterials," J. Opt. Soc. Am. B **36**(3), 559–564 (2019).
18. C. Wu, A. Salandrino, X. Ni, and X. Zhang, "Electrodynamical light trapping using whispering-gallery resonances in hyperbolic cavities," Phys. Rev. X **4**(2), 021015 (2014).
19. A. Díaz-Rubio, J. Carbonell, D. Torrent, and J. Sánchez-Dehesa, "Low-q whispering gallery modes in anisotropic metamaterial shells," Phys. Rev. B **88**(11), 115118 (2013).
20. C. F. Bohren and D. R. Huffman, *Absorption and scattering of light by small particles* (John Wiley & Sons, 2008).
21. H. C. Hulst and H. C. van de Hulst, *Light scattering by small particles* (Courier Corporation, 1981).
22. C. Díaz-Aviñó, M. Naserpour, and C. J. Zapata-Rodríguez, "Optimization of multilayered nanotubes for maximal scattering cancellation," Opt. Express **24**(16), 18184–18196 (2016).
23. W. Liu, R. F. Oulton, and Y. S. Kivshar, "Geometric interpretations for resonances of plasmonic nanoparticles," Sci. Rep. **5**(1), 12148 (2015).
24. R. Li, B. Zheng, X. Lin, R. Hao, S. Lin, W. Yin, E. Li, and H. Chen, "Design of ultracompact graphene-based superscatterers," IEEE J. Sel. Top. Quantum Electron. **23**(1), 130–137 (2017).
25. J. Dionne, H. Ashwath, and L. Kuznetsova, "Subwavelength silicon disk whispering-gallery-mode microcavities for size-dependent nanoparticles detection in the mid-infrared," Opt. Eng. **56**(5), 057111 (2017).
26. H. Chen and L. Gao, "Anomalous electromagnetic scattering from radially anisotropic nanowires," Phys. Rev. A **86**(3), 033825 (2012).

Optics EXPRESS

27. H. Chen and L. Gao, "Tunablity of the unconventional fano resonances in coated nanowires with radial anisotropy," Opt. Express **21**(20), 23619–23630 (2013).
28. A. Mirzaei, A. E. Miroshnichenko, I. V. Shadrivov, and Y. S. Kivshar, "All-dielectric multilayer cylindrical structures for invisibility cloaking," Sci. Rep. **5**(1), 9574 (2015).
29. Z. Yu, Z. Yang, Y. Wang, H. Si, and G. Zhao, "Optimized cloaks made of near-zero materials for different-sized concealed targets," Sci. Rep. **8**(1), 16739 (2018).
30. Y. Huang, Y. Feng, and T. Jiang, "Electromagnetic cloaking by layered structure of homogeneous isotropic materials," Opt. Express **15**(18), 11133–11141 (2007).
31. M. Silveirinha and N. Engheta, "Tunneling of electromagnetic energy through subwavelength channels and bends using ε-near-zero materials," Phys. Rev. Lett. **97**(15), 157403 (2006).
32. N. Kinsey, C. DeVault, A. Boltasseva, and V. M. Shalaev, "Near-zero-index materials for photonics," Nat. Rev. Mater. **4**(12), 742–760 (2019).

131.112.161.20 {ts '2020-02-18 03:07:25'}